The Eighth International Conference on Computational Fluid Dynamics (ICCFD8), Chengdu, Sichuan, China, July 14-18, 2014

ICCFD8-2014-xxxx

High Order Numerical Methods for LES of Turbulent Flows with Shocks

D.V. Kotov[1], H.C. Yee[2]*, A. Hadjadj[3], A. Wray[2], B. Sjögreen[4]

[1]Center for Turbulence Research, Stanford University, Stanford, CA 94305, USA
[2]NASA Ames Research Center, Moffett Field, CA, 94035, USA
[3]CORIA UMR 6614 & INSA de Rouen, 76800 St-Etienne du Rouvray, France
[4]Lawrence Livermore National Laboratory, Box 808, L-422, Livermore, CA 94551, USA

Abstract: Simulation of turbulent flows with shocks employing explicit subgrid-scale (SGS) filtering may encounter a loss of accuracy in the vicinity of a shock. In this work we perform a comparative study of different approaches to reduce this loss of accuracy within the framework of the dynamic Germano SGS model. One of the possible approaches is to apply Harten's subcell resolution procedure to locate and sharpen the shock, and to use a one-sided test filter at the grid points adjacent to the exact shock location. The other considered approach is local disabling of the SGS terms in the vicinity of the shock location. In this study we use a canonical shock-turbulence interaction problem for comparison of the considered modifications of the SGS filtering procedure. For the considered test case both approaches show a similar improvement in the accuracy near the shock.

Keywords: High order low dissipative scheme, Germano model, LES filtering, DNS, Subcell resolution scheme, Shock/Turbulence interaction

1 Introduction

The presence of a shock wave in turbulent flows might pose a numerical accuracy problem in employing the SGS filtered equations across shocks, depending on the LES model, the grid size, as well as the shock strength. Since the majority of dynamic LES models involve filter operations, hereafter referred to as "LES filters" to distinguish them from standard "numerical filters", when the LES filtered equations are applied through the shock, the Rankine-Hugoniot relations are affected by the filtering operation, since the filtered variables are not discontinuous. In the present study we consider LES with implicit filtering employing the dynamic Germano procedure [1] for calculating the model coefficients. The dynamic Germano procedure was developed for shock free turbulence. Sagaut and Germano [2] have noticed that the usual filtering procedures, based on a central spatial filter that provides information from both sides, when applied around the shock, produce parasitic contributions that affect the filtered quantities. They suggested using non-centered filters to avoid this nonphysical effect. In [3] shock-confining filters have been proposed instead. Another approach based on the deconvolution method is considered in [4].

Aside from the subgrid scale filtering procedure, the accuracy of LES with shocks depends heavily on the accuracy of the numerical scheme. In this study we consider a combination of the low dissipative high order nonlinear filter scheme of Yee and Sjögreen [5] to locate the shock accurately, and the subcell resolution method of Harten [6] to confine the shock location to be within a grid cell. Previous studies indicate that the combination of the nonlinear filter scheme with Harten's subcell resolution method is able to accurately locate the shock within a grid cell. For the comparison we will also consider a modification of the SGS

*Corresponding author's email: helen.m.yee@nasa.gov

filtering procedure including local one-sided filtering without subcell resolution. One more modification considered here is local disabling of subgrid-scale (SGS) dissipation, which has been employed in previous studies [7, 8]. A new method to handle the transition points (buffer zone) between the smeared shock and the one-sided SGS filter equations is under development.

The outline of the paper is as follows. Section 2 provides a description of the LES model considered and the numerical scheme used to solve the governing equations with the details on the three modifications of the LES filtering procedure. Section 3 describes the shock-turbulence interaction problem setup and a comparison of the the current DNS computations with the digitized results from [9]. Then LES computations employing the proposed method are compared with the filtered DNS data, and with LES results using standard and modified LES filtering procedures.

2 Mathematical Formulation and Numerical Methods

2.1 Governing Equations and LES Model

We consider the filtered compressible Navier-Stokes equations written in the conservative form

$$\begin{aligned} \partial_t \bar{\rho} + \partial_j(\bar{\rho}\tilde{u_j}) &= 0 && (1)\\ \partial_t(\bar{\rho}\tilde{u_i}) + \partial_j(\bar{\rho}\tilde{u_i}\tilde{u_j} + \bar{p}\delta_{ij} - \check{\tau}_{ij} + \tau^S_{ij}) &= 0 && (2)\\ \partial_t(\bar{\rho}\tilde{E}) + \partial_j(\bar{\rho}\tilde{E}\tilde{u_j} + \bar{p}\tilde{u_j} - \check{\tau}_{ij}\tilde{u}_i + \check{q}_j + q^S_j) &= 0, && (3) \end{aligned}$$

where ρ is the density, u_i is the i^{th} velocity component, p is the pressure, T is the temperature, E is the total energy, and t is the time. For a function f, the LES filtering operation is denoted as $\bar{f}$:

$$\bar{f}(\mathbf{r},t) = \frac{1}{\Delta}\int_{-\infty}^{\infty}\int_{-\infty}^{\infty} G\left(\tfrac{\mathbf{r}-\xi}{\Delta}, t-\tau\right) f(\xi,\tau)d\xi d\tau, \quad (4)$$

where $G(x,t)$ is the filter kernel in physical space and Δ is the filter width. The Favre filtering operation is denoted as $\tilde{f} = \overline{\rho f}/\bar{\rho}$, and $\check{f}$ stands for the Favre-filtered variables:

$$\check{\tau}_{ij} = 2\mu(\tilde{T})(\tilde{S}_{ij} - \frac{1}{3}\delta_{ij}\partial_k\tilde{u}_k), \quad \tilde{S}_{ij} = (\partial_j\tilde{u}_i + \partial_i\tilde{u}_j)/2 \quad (5)$$

$$\check{q}_j = -\lambda(\tilde{T})\partial_j\tilde{T}. \quad (6)$$

Unlike the "bar" and "tilde", the "breve" symbol does not denote a filtering operation, but indicates that the quantity is based on primitive filtered variables. In the equations (5) and (6) the dynamic viscosity is given by $\mu(T) = \mu_0(T/T_0)^{3/4}$ and thermal conductivity is expressed through a constant Prandtl number Pr and heat capacity at constant pressure c_p: $\lambda(T) = c_p\mu(T)/Pr$. The equation of state is $\bar{p} = R\bar{\rho}\tilde{T}$, where R is the gas specific constant. The subgrid-scale (SGS) terms, SGS stress tensor τ^S_{ij}, and SGS heat flux q^S_j are modeled as follows:

$$\begin{aligned} \tau^S_{ij} - \frac{1}{3}\tau^S_{kk}\delta_{ij} &= -2\mu_t(\tilde{S}_{ij} - \frac{1}{3}\tilde{S}_{kk}\delta_{ij}) && (7)\\ \tau^S_{kk} &= 2C_I\bar{\rho}\Delta^2|\tilde{S}|^2 && (8)\\ q^S_j &= \frac{\mu_t\gamma c_v}{Pr_t}\partial_j\tilde{T}, && (9) \end{aligned}$$

where $\mu_t = \bar{\rho}C_s\Delta^2|\tilde{S}|$, and $|\tilde{S}| = \sqrt{2\tilde{S}_{ij}\tilde{S}_{ij}}$. The Smagorinsky constant C_s and the constant for the isotropic part of the SGS stress C_I are obtained through Germano-Lilly [10] procedure:

$$C_s = \frac{\left\langle L^{C_s}_{ij} M^{C_s}_{ij}\right\rangle_H}{\left\langle M^{C_s}_{ij} M^{C_s}_{ij}\right\rangle_H}, \qquad C_I = \frac{\langle L_{ll}\rangle_H}{\left\langle M^{C_I}_{ll}\right\rangle_H}, \quad (10)$$

where

$$L_{ij}^{C_s} = L_{ij} - \frac{1}{3}L_{ll}\delta_{ij}, \qquad L_{ij} = \left(\widehat{\bar{\rho}\tilde{u}_i\tilde{u}_j}\right) - \widehat{\bar{\rho}\tilde{u}_i}\widehat{\bar{\rho}\tilde{u}_j}/\hat{\bar{\rho}} \tag{11}$$

$$M_{ij}^{C_s} = -2\hat{\bar{\rho}}\hat{\Delta}^2|\hat{\tilde{S}}|^2\left(\widehat{\tilde{S}_{ij} - \frac{1}{3}\tilde{S}_{ll}\delta_{ij}}\right) + 2\Delta^2\left[\left(\widehat{\bar{\rho}|\tilde{S}|\tilde{S}_{ij}}\right) - \frac{1}{3}\left(\widehat{\bar{\rho}|\tilde{S}|\tilde{S}_{ll}}\delta_{ij}\right)\right] \tag{12}$$

$$M_{ll}^{C_I} = 2\hat{\bar{\rho}}\hat{\Delta}^2|\hat{\tilde{S}}|^2 - 2\Delta^2\left(\widehat{\bar{\rho}|\tilde{S}|^2}\right) \tag{13}$$

and $< f >_H$ stands for averaging in homogeneous (periodic) directions.

For the considered test case with low turbulent Mach number $M_t < 0.4$ it is shown [11] that the isotropic part of the SGS stress can be neglected: $C_I = 0$. The Germano procedure requires an explicit test filtering operation, denoted here with the hat symbol. For the Germano procedure we use a 3D filtering operator based on a 1D trapezoidal filter:

$$\hat{f}_i = \frac{1}{4}f_{i-1} + \frac{1}{2}f_i + \frac{1}{4}f_{i+1}. \tag{14}$$

Note that according to [12] the width of the discrete filter can be estimated as

$$\Delta = h\sqrt{12\sum_{j=-(N-1)/2}^{(N-1)/2} j^2 W_j}, \tag{15}$$

where h is the grid spacing and W_j are the filter weights. Using formula (15) for filter (14) gives $\Delta = h\sqrt{6}$.

2.2 High-Order Filter Schemes

In order to solve the system (1) – (3) introducing as little numerical dissipation as possible, we use the high-order nonlinear filter scheme of Yee *et al.* [5, 13, 14, 15] which consists of three steps.

2.2.1 Preprocessing Step

Before the application of a high-order non-dissipative spatial base scheme, a preprocessing step is employed to improve the stability. The inviscid flux derivatives of the governing equations are split into the following three ways, depending on the flow types and the desire for rigorous mathematical analysis or physical argument.

- Entropy splitting of [16] and [17, 18]. The resulting form is non-conservative and the derivation is based on entropy norm stability with boundary closure for the initial value boundary problem.
- The system form of the [19] splitting. This is a conservative splitting and the derivation is based on physical arguments.
- Tadmor entropy conservation formulation for systems [20]. The derivation is based on mathematical analysis. It is a generalization of Tadmor's entropy formulation to systems and has not been fully tested on complex flows.

For the current test case containing a shock wave in the flow field it is more appropriate to use a conservative splitting. The Ducros et al. splitting is employed for all the computations.

2.2.2 Base Scheme Step

A full time step is advanced using a high-order non-dissipative (or very low dissipation) spatially central scheme on the split form of the governing partial differential equations (PDEs). A summation-by-parts (SBP) boundary operator [21, 22] and matching order conservative high-order free stream metric evaluation for curvilinear grids [23] are used. High-order temporal discretization such as the third-order or fourth-order Runge-Kutta (RK3 or RK4) method is used. It is remarked that other temporal discretizations can be used for the base scheme step.

2.2.3 Post-Processing (Nonlinear Filter Step)

To further improve nonlinear stability from the non-dissipative spatial base scheme, after the application of a non-dissipative high-order spatial base scheme on the split form of the governing equation(s), the post-processing step is used to nonlinearly filter the solution by a dissipative portion of a high-order shock-capturing scheme with a local flow sensor. The flow sensor provides locations and amounts of built-in shock-capturing dissipation that can be further reduced or eliminated. At each grid point a local flow sensor is employed to analyze the regularity of the computed flow data. Only the discontinuity locations would receive the full amount of shock-capturing dissipation. In smooth regions no shock-capturing dissipation would be added. In regions with strong turbulence, if needed, a small fraction of the shock-capturing dissipation would be added to improve stability. For a variety of local flow sensors with automatic selection of the proper parameter, depending on different flow types see [13]. For the problem considered in this work we use Ducros *et al.* flow sensor [24]:

$$w = \frac{(\nabla \cdot \mathbf{u})^2}{(\nabla \cdot \mathbf{u})^2 + \omega^2 + \varepsilon}. \tag{16}$$

Here $\mathbf{u}$ is velocity vetor, ω is vorticity magnitude and $\varepsilon = 10^{-6}$ is a small number to avoid division by zero. The nonlinear dissipative portion of a high-resolution shock-capturing scheme can be any shock-capturing scheme. For the problem considered in this study it is activated when the Ducros *et al.* sensor $w > 0.6$ for the case $M = 1.5$ and $w > 0.3$ for the case $M = 3$.

Let U^* be the solution after the completion of the base scheme step. The final update of the solution after the filter step is (with the numerical fluxes in the y- and z-directions suppressed as well as their corresponding y- and z-direction indices on the x inviscid flux suppressed)

$$U^{n+1}_{j,k,l} = U^*_{j,k,l} - \frac{\Delta t}{\Delta x}[H^*_{j+1/2} - H^*_{j-1/2}], \quad H_{j+1/2} = R_{j+1/2}\overline{H}_{j+1/2}, \tag{17}$$

where $R_{j+1/2}$ is the matrix of right eigenvectors of the Jacobian of the inviscid flux vector in terms of Roe's average states based on U^*. $H^*_{j+1/2}$ and $H^*_{j-1/2}$ are "filter" numerical fluxes in terms of Roe's average states based on U^*. Denote the elements of the filter numerical flux vector $\overline{H}_{j+1/2}$ by $\overline{h}^l_{j+1/2}, l = 1, 2, ..., 5$. The nonlinear portion of the filter numerical flux $\overline{h}^l_{j+1/2}$ has the form

$$\overline{h}^l_{j+1/2} = \frac{\kappa}{2} w^l_{j+1/2} \phi^l_{j+1/2}. \tag{18}$$

Here $w^l_{j+1/2}$ is a flow sensor to activate the nonlinear numerical dissipation portion of a high order shock-capturing scheme $\frac{1}{2}\phi^l_{j+1/2}$, and κ is a positive parameter that is less than or equal to one. The choice of the parameter κ can be different for different flow types and is automatically chosen by using the local κ described in [13]. However, in this study we set $\kappa = 1$ to be used with the standard Durcos et al. flow sensor.

It is noted that the nonlinear filter step described above should not be confused with the LES filtering operation. For previous studies on the performance of this filter scheme in DNS and LES simulations, see [14, 25, 26, 27, 28, 29, 13, 15]. This scheme has been validated for DNS of a 3D channel flow, 2D temporal and spatial evolving mixing layers, Richtmyer-Meshkov instability, 3D Taylor-Green vortex, 3D isotropic turbulence with shocklets, extreme condition flows, and 3D LES of temporal evolving mixing layers comparing with experimental data.

2.3 Modifications of the LES Filtering Procedure for Flows with Shocks

During LES computation using the filtered governing equations, there are two additional sources of inaccuracy that may appear near the shock. The first one is connected with the numerical scheme used for solving the governing equations. Away from the shock the high-order central scheme is applied, introducing a negligible amount of numerical dissipation. However, in the vicinity of the shock the shock-capturing scheme is activated, introducing numerical dissipation into the computed solutions. The amount of numerical dissipation introduced by the shock capturing scheme depends on the particular problem parameters and may be higher than the turbulent dissipation modeled by the SGS terms. Hadjadj and Barmeo [7, 8] proposed to locally disable the SGS terms in order to obtain more accurate results. Denote this procedure as LES-Z:

Procedure LES-Z

1. *Employ flow sensor to detect shocks*
2. *Obtain C_s from Dynamic Germano Procedure except near the shock*
3. *Set $C_s = 0$ within grid stencil width of the scheme at shock*

Setting $C_s = 0$ within the grid stencil width of the shock location (according to the computed flow sensor indicator) might appears to be too abrupt. An alternate procedure would be to set $C_s = 0$ at the shock location and a smooth transition function C_s such as *tanh* in the vicinity of the shock. Our studies show that setting $C_s = 0$ for the whole WENO grid stencil width rather than a *tanh* smoothing function produces better results.

The second additional source of inaccuracy of LES results in the vicinity of the shock comes from the fact that the explicit filtering operation in (10) – (13) is applied across the shock, causing inaccuracy of the results. In this case, as is pointed out in [2], a one-sided filtering operation should be used instead of a central form. Denote this procedure as LES-1S:

Procedure LES-1S

1. *Employ flow sensor to detect shocks*
2. *Employ Harten's subcell resolution approach to detect exact shock location*
3. *Obtain C_s from Dynamic Germano Procedure except near the shock*
4. *Apply one-sided filtering procedure to the left and right of the shock location*

It is noted that for the one-sided filtering formulation, one should use a discrete filter with the same filter width as in the standard central filter procedure. For example, with the trapezoidal filter (14) one can use the right-sided filter $\hat{f}_i^+ = \frac{1}{2} f_i + \frac{1}{2} f_{i+1}$, which according to formula (15) has the same $\Delta = h\sqrt{6}$ as filter (14).

The third considered modification is based on Harten's subcell resolution (SR) approach [6] combined with ENO reconstruction. Any shock-capturing method applied at the shock will result in smearing the shock. By estimating the exact shock location through SR and using ENO reconstruction one can sharpen the shock so that the numerical dissipation is minimized more locally. Denote this procedure as LES-SR:

Procedure LES-SR

1. *Employ flow sensor to detect shocks*
2. *Employ Harten's SR approach to detect exact shock location*
3. *Obtain C_s from Dynamic Germano Procedure except near the shock*
4. *Employ ENO reconstruction for the values of the points adjacent to the shock*
5. *Apply one-sided filtering procedure to the left and right of the shock location*

3 3D Turbulence Across a Supersonic Shock Wave

3.1 Problem Setup

The 3D test case considered here concerns an initial turbulence disturbance at inflow boundary interacting with a stationary supersonic planar shock wave. The problem has been studied by previous investigators, mainly related to DNS computations, e.g. [30, 9, 8]. Here we choose the configuration considered in the DNS study of [9]. Figure 1 shows a schematic of the problem setup. The computational domain limits are $-2 \le x \le -2 + 4\pi$, $0 \le y \le 2\pi$ and $0 \le z \le 2\pi$. The grid is uniform in all directions with the spacing in x three times finer than in y and z (see [9] for explanation). We solve the filtered governing equations (1) – (3) in a non-dimensional form. The Yee *et al.* filter scheme with Ducros *et al.* flow sensor [24] is used for integration of the governing equations. The spatial base scheme is the 8th-order central differencing and the nonlinear filter scheme is the dissipative portion of the 7th-order WENO scheme. Since the initial data consists of a planar shock in the x-direction, numerical dissipation should be mainly needed in the x-direction. In order to obtain more accurate results WENO dissipation is employed only in the x direction at the postprocessing stage of the Yee *et al.* filter. The inflow and outflow boundary conditions are applied in the streamwise direction and periodic boundary conditions are applied in the transverse directions.

Inflow boundary condition. A fully developed turbulent inflow condition is applied using a turbulent database. This database is generated as follows. First, an initial isotropic turbulent field with the energy

spectrum $E(k) \sim k^4 \exp(-2k^2/k_0^2)$ and microscale Reynolds number $Re_\lambda = \rho\lambda u'_{rms}/\mu = 140$ is generated using the methodology described in [31]. Here the energy peak wavenumber $k_0 = 4$ is used. Next, the decay of this field in a periodic box is simulated for approximately three eddy turnover times $\tau = \lambda/u'_{rms}$ to ensure fully developed turbulence. After the decay the Reynolds number $Re_\lambda = 40$ and the turbulent Mach number is $M_t = \overline{u'_i u'_i}^{1/2}/c_0 = 0.16$. Here c_0 is the mean speed of sound. The generated isotropic turbulence is introduced at the inflow boundary with constant mean velocity u_0. We consider two cases with mean flow Mach number $M = 1.5$ and $M = 3.0$. In order to compare the DNS results we use the inflow database from [9].

Outflow boundary condition. In order to avoid acoustic reflections of subsonic flow from the outflow boundary a non-reflective sponge layer is employed on the region near the outflow. The length of this layer is $x_{max} - x_{sp} = \pi$. The sponge layer is implemented by introducing a following source term into the equations (1) – (3)

$$\Omega = -\frac{k_0 u_0}{2\pi}\left(\frac{x - x_{sp}}{x_{max} - x_{sp}}\right)(f - < f >_{yz}), \tag{19}$$

where $f = \rho, \rho u_i, \rho E$ and $\langle\cdot\rangle_{yz}$ denotes averaging in the y- and z- directions.

The outflow pressure p_∞ is chosen such that the mean shock location is stationary. For laminar flow Rankine-Hugoniot conditions give

$$\frac{p_\infty}{p_0} = 1 + \frac{2\gamma}{\gamma + 1}\left[\frac{(u_0 - U_s)^2}{c_0^2} - 1\right], \tag{20}$$

where p_0 is the inflow mean pressure, u_0 is the mean inflow velocity, c_0 is the mean inflow speed of sound and U_s is the shock velocity. As the inflow condition is turbulent, the Rankine-Hugoniot conditions are valid only instantaneously but not in average. After an initial guess based on (20) the outflow pressure is refined by an iteration procedure, integrating the governing equations on a coarse grid and updating the pressure according to the formula

$$p'_\infty = p_\infty + 4U_s\rho_u u_0/(\gamma + 1). \tag{21}$$

See [9] for more details.

Gathering statistics. The simulation statistics for a given function f are obtained by averaging in time and in homogeneous directions:

$$< f >_H (x) = \frac{1}{L_y L_z \Delta t}\int_{t_0}^{t_0+\Delta t}\int_0^{L_y}\int_0^{L_z} f(\mathbf{r}, t)dzdydt, \tag{22}$$

where L_y and L_z are domain sizes in transverse directions. The averaging is performed over a time span $\Delta t \approx 100/(k_0 u_0)$. Convergence is confirmed by comparing the results with statistics obtained over time span $\Delta t/2$. The statistics are gathered after the transition period has passed. Transient time t_0 is estimated as $t_0 \gg L_x/u_0$, where L_x is the domain size in the streamwise direction. The correct choice of transient time is confirmed by comparing with the statistics obtained starting from time $t_0/2$.

3.2 DNS Comparison

After a grid refinement study the DNS results as a reference solution for LES comparison are obtained on a grid with 1553×256^2 points. The instantaneous streamwise and transverse velocity fields are shown in Fig. 2. During the computation over a long time evolution, the shock slightly moved upstream. For this turbulent Mach number the shock is wrinkled due to turbulent inflow. As shown in previous studies [30, 9], the shock may break at higher turbulent Mach numbers M_t. The turbulence is compressed by the shock, and immediately behind the shock it is anisotropic. The comparison of turbulent statistics for streamwise and transverse components of the vorticity and Reynolds stress shows that the turbulence becomes isotropic again downstream of $x \approx 3$. Downstream of $x = 8$ turbulence is essentially damped with the sponge source term.

Figures 3 – 6 represent the DNS statistics for different cases. The plots are presented in the reference frame of the average shock location.

The comparison of the DNS statistics obtained in this work using the *ADPDIS3D* [5] code with the

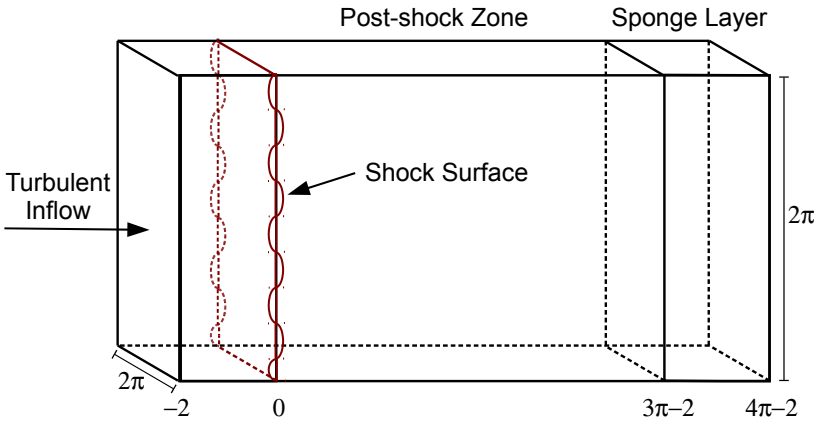

Figure 1: Turbulence across a shock wave problem setup.

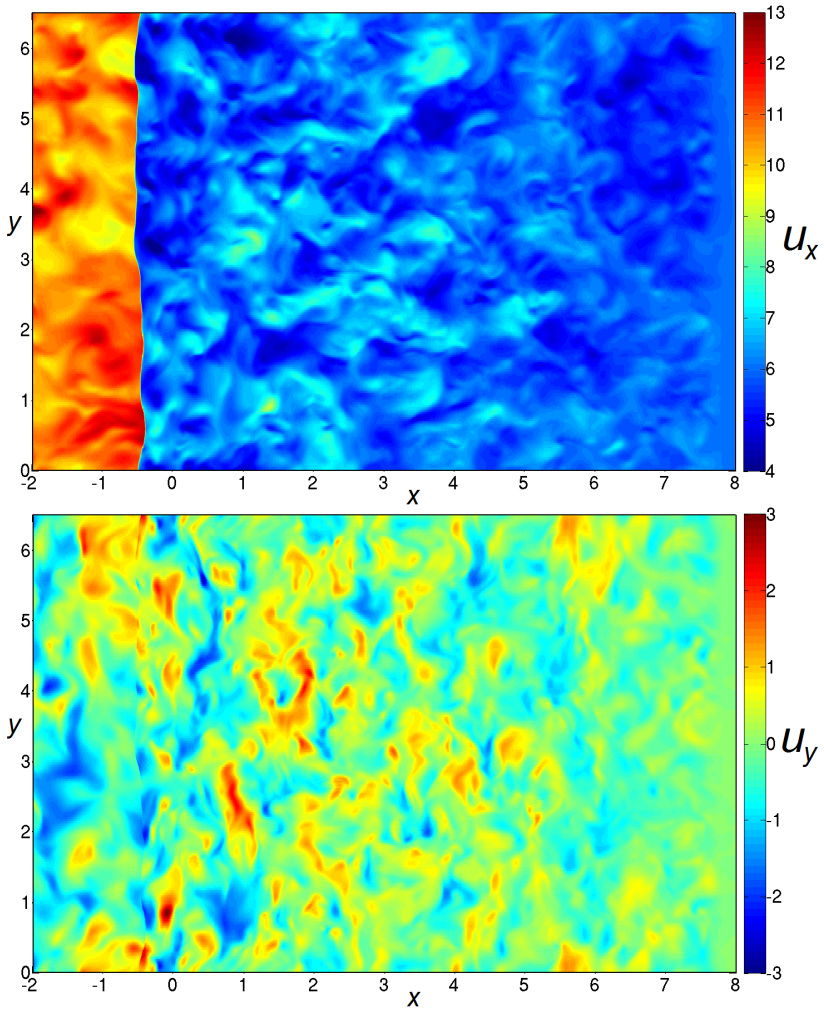

Figure 2: Instantaneous velocity field u_x (top) and u_y (bottom) obtained with DNS on grid of 1553×256^2 points. Slice $z = \text{const}$.

data obtained from digitizing the solution [9] are shown in Fig. 3. The results are in good agreement. The grid resolution in the vicinity of the shock is the same. In [9] grid clustering near the shock has been employed, resulting in a smaller grid size, 694×256^2. The work [9] employs the *HYBRID* code, which also uses a Ducros *et al.* flow sensor for shock detection. However, in [9] WENO dissipation has been introduced at every Runge-Kutta stage, whereas the Yee *et al.* scheme allows decreasing the computational cost by employing WENO dissipation only after the full Runge-Kutta step.

The results of the grid refinement study for cases $M = 1.5$ and $M = 3$ on levels of grid refinement are shown in Figs. 4 and 5. For the case $M = 1.5$ the results on 777×128^2 are fairly close to the DNS results obtained with 1553×256^2 grid points, especially for the Reynolds stress statistics. For the case $M = 3$ the results also converge, but the convergence is slower.

The comparison between the filtered DNS data and the results obtained with different numerical schemes on the coarse grid with 389×64^2 points is shown in Fig. 6. Here we compare the results obtained by WENO of 5^{th} order (WENO5) and WENO of 7^{th} order (WENO7) with the results obtained by the filter counterpart of WENO7 with Ducros *et al.* split (WENO7fi+split). For DNS on a coarse grid a too low-dissipative scheme will produce inaccurate results. To obtain the results by the filter scheme shown in Fig. 6, we use WENO dissipation in all directions. It is noted that for LES simulation it is more important to use a low-dissipative scheme, since the dissipation is already introduced by the turbulence model.

3.3 LES Comparison

In this section we compare the results obtained by the Germano model using different filtering procedures (LES with standard filtering procedure, LES-Z, and LES-1S) with the DNS solution filtered to the size of the LES grid. Results obtained by LES-SR are not shown, since that method is still under development.

Comparison of the methods on a grid with 389×64^2 points for the case $M = 1.5$ is shown in Figs. 8 and 9. For this case the results obtained using LES-Z and LES-1S are closer to the filtered DNS than standard LES. For certain variables, LES-1S performs slightly better than LES-Z. However, the difference between LES-1S and LES-Z may be more significant for other flow conditions, e.g., higher Mach and turbulent Mach numbers. In the case when the shock-capturing scheme dissipation might be larger than the SGS dissipation, it is conjectured that LES-Z would be more accurate than the other considered approach. But for the cases where the SGS dissipation is larger than the numerical scheme dissipation, LES-1S might obtain more accurate results than LES-Z.

The results for the same case on a two-times finer grid (777×128^2) are shown in Fig. 10. All results obtained on this grid are quite close to each other, though LES without any modification of the filtering procedure is slightly closer to the filtered DNS data. One can assume that the shock is resolved enough at this level of grid refinement so that there is no need for additional shock treatment.

A similar comparison of the methods on the grid with 389×64^2 points for the higher Mach number case ($M = 3$) is shown in Fig. 11. The behavior of the methods is similar to the $M = 1.5$ case, but LES-Z here performs slightly better than LES-1S, which can be seen especially in the plot of the y vorticity component.

It is remarked that as we employ implicitly filtered LES equations, the width of implicit filter is not well defined. One should take this fact into account when using filtered DNS data as a reference solution for verification of the LES model. Figure 12 shows the differences in filtered DNS data when using two different filters:

- the 5-point top-hat filter with coefficients $(1/8, 1/4, 1/4, 1/4, 1/8)$ and width $\Delta \approx 4.2h$ according to the estimate (15),
- the 7-point trapezoidal filter with coefficients $(1/22, 1/11, 2/11, 4/11, 2/11, 1/11, 1/22)$ and width $\Delta \approx 4.8h$.

The top-hat filter has been used to obtain DNS filtered data plotted on previous figures. For more precise comparison of LES filtering modifications, explicit LES will be considered in the future.

4 Conclusions

The DNS results obtained by high order nonlinear filter schemes compare well with the reference solution [9]. In general, the employment of the Yee & Sjögreen filter schemes requires less computational cost than

standard Hybrid schemes. Our LES study confirms the results found by previous authors that the dynamic Germano LES model with a standard filtering procedure may loose accuracy due to a strong shock. Two modifications of the LES filtering procedure (LES-Z and LES-1S) which are designed for improving the accuracy of the standard method have been considered. For this particular shock-turbulence interaction test case both modifications of the filtering procedure show similar results which are more accurate than the results obtained using the standard LES filtering procedure. However, the turbulent Mach number $M_t = 0.16$ for the test case considered here is quite low, and the SGS dissipation may be not high enough in comparison with numerical dissipation of the shock-capturing scheme. Different behavior of considered procedures is expected for high turbulent Mach numbers, which is forthcoming. In addition, a systematic assessment employing LES-SR and LES-1S will be reported in a forthcoming report. Also, for better estimation of the simulations accuracy the performance of explicitly filtered LES will be considered.

Acknowledgments

The support of the DOE/SciDAC SAP grant DE-AI02-06ER25796 is acknowledged. The authors are grateful to J. Larsson for providing the turbulent inflow and selected input data. The work has been performed with the first author as a postdoctoral fellow at the Center for Turbulence Research, Stanford University. Financial support from the NASA Aerosciences/RCA program for the second author is gratefully acknowledged. Work by the fifth author was performed under the auspices of the U.S. Department of Energy at Lawrence Livermore National Laboratory under Contract DE-AC52-07NA27344.

References

[1] M. Germano, U. Piomelli, P. Moin, and W. Cabot. A dynamic subgrid-scale eddy viscosity model. *Physics of Fluids*, 3(7):1760–1765, 1991.

[2] P. Sagaut and M. Germano. On the filtering paradigm for LES of flows with discontinuities. *J. of Turbulence*, 6(23):1–9, 2005.

[3] N. E. Grube and M. P. Martin. Assessment of subgrid-scale models and shock-confining filters in large-eddy simulation of highly compressible isotropic turbulence. *AIAA Paper*, (2009-0947), 2009.

[4] N. A. Adams and S. Stolz. A subgrid-scale deconvolution approach for shock capturing. *J. Comp. Phys.*, 178:391–426, 2002.

[5] H. C. Yee and B. Sjögreen. Development of low dissipative high order filter schemes for multiscale Navier-Stokes/MHD systems. *J. Comput. Phys.*, 225:910–934, 2007.

[6] A. Harten. ENO schemes with subcell resolution. *J. Comp. Phys.*, 83:148–184, 1989.

[7] A. Hadjadj and S. Dubos. Large eddy simulation of supersonic boundary layer at $M = 2.4$. In M. Braza and K. Hourigan, editors, *Proceeding of the IUTAM Symposium on Unsteady Separated Flows and their Control*. Springer, 2009. e-ISBN 978-1-4020-9898-7.

[8] I. Bermejo-Moreno, J. Larsson, and S. K. Lele. LES of canonical shock-turbulence interaction. *Annual Research Briefs, Center for Turbulence Research, Stanford*, 2010.

[9] J. Larsson and S. K. Lele. Direct numerical simulation of canonical shock/turbulence interaction. *Physics of Fluids*, 21(126101), 2009.

[10] D. K. Lilly. A proposed modification of the Germano subgrid-scale closure method. *Physics of Fluids*, 4(3):633–635, 1992.

[11] G. Erlebacher, M. Y. Hussaini, C. G. Speziale, and T. A. Zang. Toward the large eddy simulation of compressible turbulent flows. *J. Fluid Mech.*, 238:155, 1992.

[12] T. S. Lund. On the use of discrete fiters for large eddy simulation. *Annual Research Briefs, Center for Turbulence Research, Stanford*, 1997.

[13] H. C. Yee and B. Sjögreen. High order filter methods for wide range of compressible flow speeds. In *Proc. of ICOSAHOM 09*, Trondheim, Norway, June 22-26 2013.

[14] H. C. Yee, N.D. Sandham, and M.J. Djomehri. Low dissipative high order shock-capturing methods using characteristic-based filters. *J. Comput. Phys.*, 150:199–238, 1999.

[15] D. Kotov, H. C. Yee, and B. Sjögreen. Performance of improved high-order filter schemes for turbulent flows with shocks. *Annual Research Briefs, Center for Turbulence Research, Stanford*, 2013.

[16] P. Olsson and J. Oliger. Energy and maximum norm estimates for nonlinear conservation laws. Technical Report 94.01, RIACS, 1994.

[17] H. C. Yee, M. Vinokur, and M.J. Djomehri. Entropy splitting and numerical dissipation. *J. Comput. Phys.*, 162:33–81, 2000.

[18] H.C. Yee and B. Sjögreen. Designing adaptive low dissipative high order schemes for long-time integrations. In D. Drikakis & B. Geurts, editor, *Turbulent Flow Computation*. Kluwer Academic, 2002.

[19] F. Ducros, F. Laporte, T. Soulères, V. Guinot, P. Moinat, and B. Caruelle. High-order fluxes for conservative skew-symmetric-like schemes in structured meshes: Application to compressible flows. *J. Comp. Phys.*, 161:114–139, 2000.

[20] B. Sjögreen and H. C. Yee. On skew-symmetric splitting and entropy conservation schemes for the euler equations. In *Proc. of the 8th Euro. Conf. on Numerical Mathematics & Advanced Applications (ENUMATH 2009)*, Uppsala, Sweden, June 29 - July 2 2009. Uppsala University.

[21] P. Olsson. Summation by parts, projections, and stability. I. *Math. Comp.*, 64:1035–1065, 1995.

[22] B. Sjögreen and H. C. Yee. On tenth-order central spatial schemes. In *Proceedings of the Turbulence and Shear Flow Phenomena 5 (TSFP-5)*, Munich, Germany, August 27-29 2007.

[23] M. Vinokur and H. C. Yee. Extension of efficient low dissipative high-order schemes for 3-d curvilinear moving grids. In *Frontiers of Computational Fluid dynamics*, pages 129–164. World Scientific, 2002.

[24] F. Ducros, V. Ferrand, F. Nicoud, C. Weber, D. Darracq, C. Gacherieu, and T. Poinsot. Large-eddy simulation of the shock/turbulence interaction. *J. Comput. Phys.*, 152:517–549, 1999.

[25] N. D. Sandham, Q. Li, and H. C. Yee. Entropy splitting for high-order numerical simulation of compressible turbulence. *J. Comp. Phys.*, 178:307–322, 2002.

[26] B. Sjögreen and H. C. Yee. Multiresolution wavelet based adaptive numerical dissipation control for shock-turbulence computation. *J. Sci. Comput.*, 20:211–255, 2004.

[27] H. C. Yee and B. Sjögreen. Simulation of Richtmyer-Meshkov instability by sixth-order filter methods. *Shock Waves*, 17:185–193, 2007.

[28] H. C. Yee, B. Sjögreen, and A. Hadjadj. Comparative study of three high order schemes for LES of temporally evolving mixing layers. *Commun. Comput. Phys.*, 12:1603–1622, 2012.

[29] A. Hadjadj, H. C. Yee, and B. Sjögreen. LES of temporally evolving mixing layers by an eighth-order filter scheme. *Int. J. for Num. Meth. in Fluids*, 70:1405–1427, 2012.

[30] S. Lee, S. K. Lele, and P. Moin. Interaction of isotropic turbulence with shock waves: effect of shock strength. *J. Fluid Mech.*, 340:225–247, 1997.

[31] J. R. Ristorcelli and G. A. Blaisdell. Consistent initial conditions for the DNS of compressible turbulence. *Physics of Fluids*, 9(4), 1997.

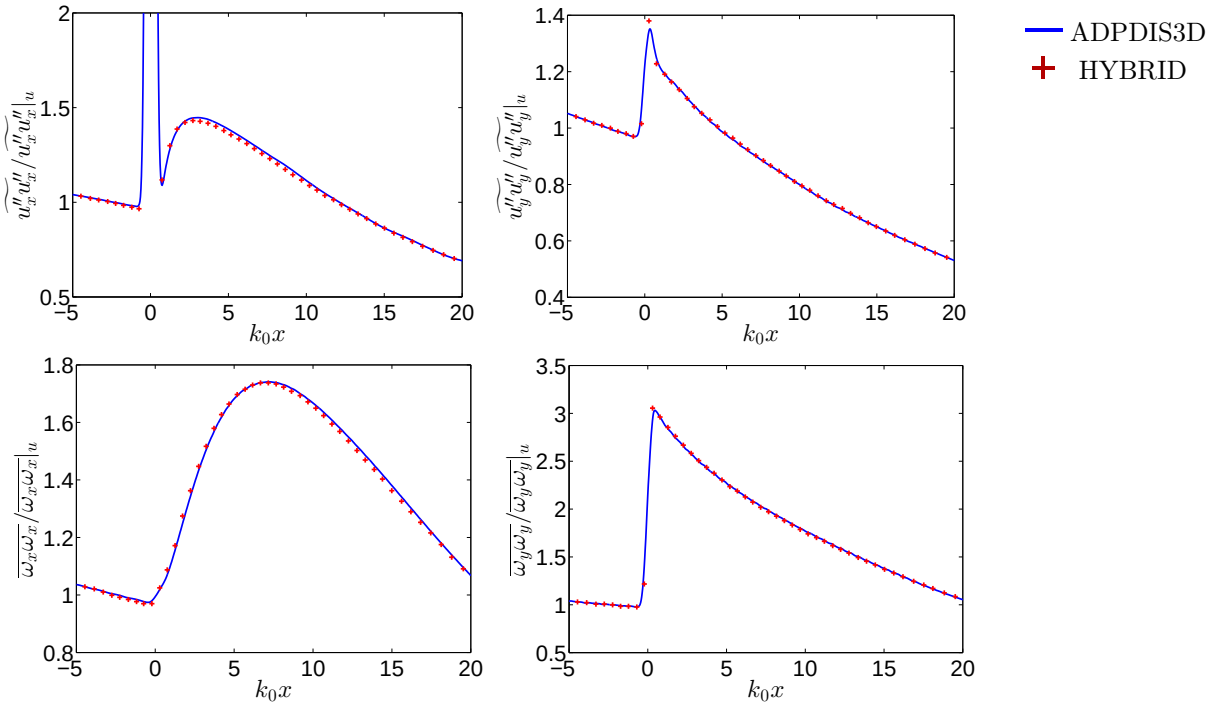

Figure 3: Comparison of DNS statistics obtained in this work employing the *ADPDIS3D* code with data obtained from digitizing the solution [9] employing the *HYBRID* code. Top row: Reynolds Stress components x (left) and y (right). Bottom row: vorticity components x (left) and y (right).

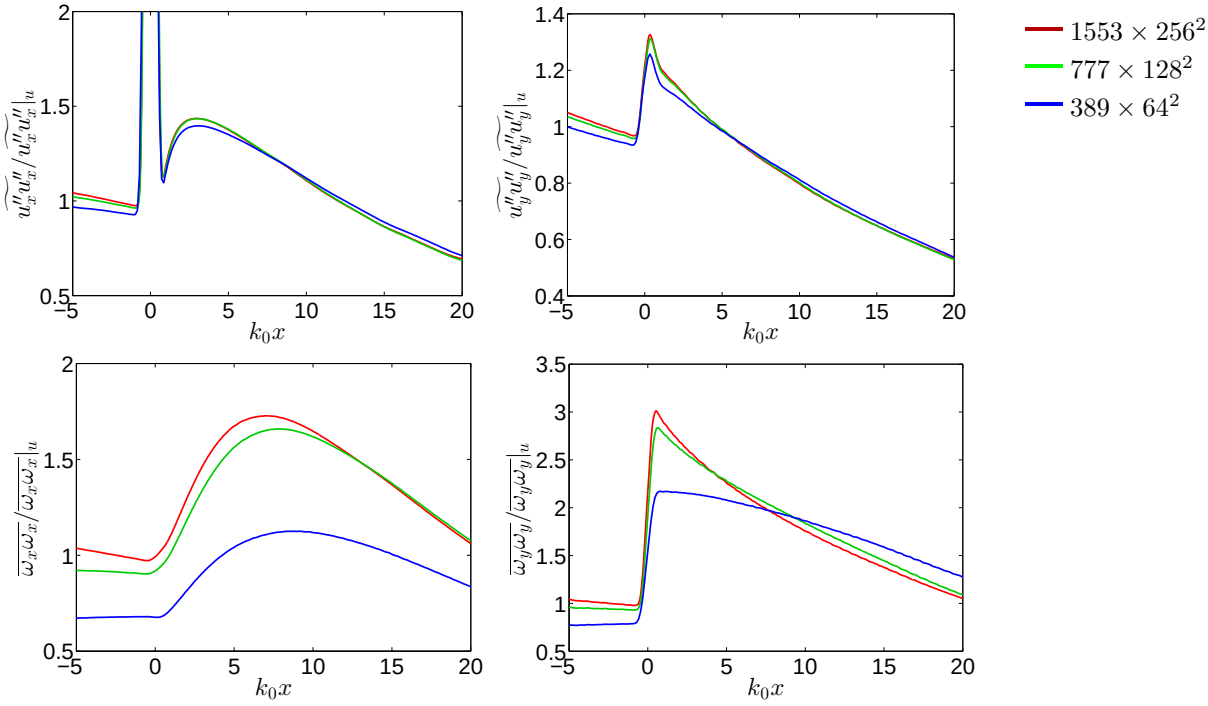

Figure 4: Grid refinement study for the case $M = 1.5$ on three grid levels: 389×64^2, 777×128^2 and 1553×256^2. Top row: Reynolds Stress components x (left) and y (right). Bottom row: vorticity components x (left) and y (right). No LES modeling.

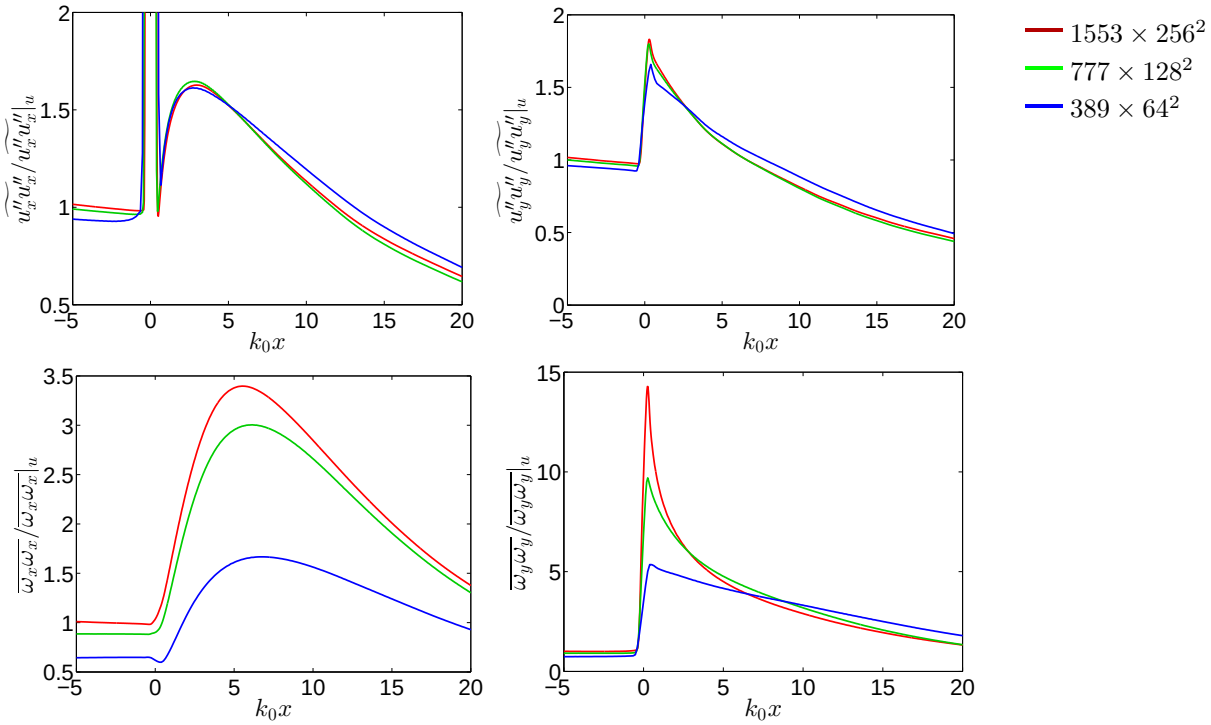

Figure 5: Grid refinement study for the case $M = 3$ on three grid levels: 389×64^2, 777×128^2 and 1553×256^2. Top row: Reynolds Stress components x (left) and y (right). Bottom row: vorticity components x (left) and y (right). No LES modeling.

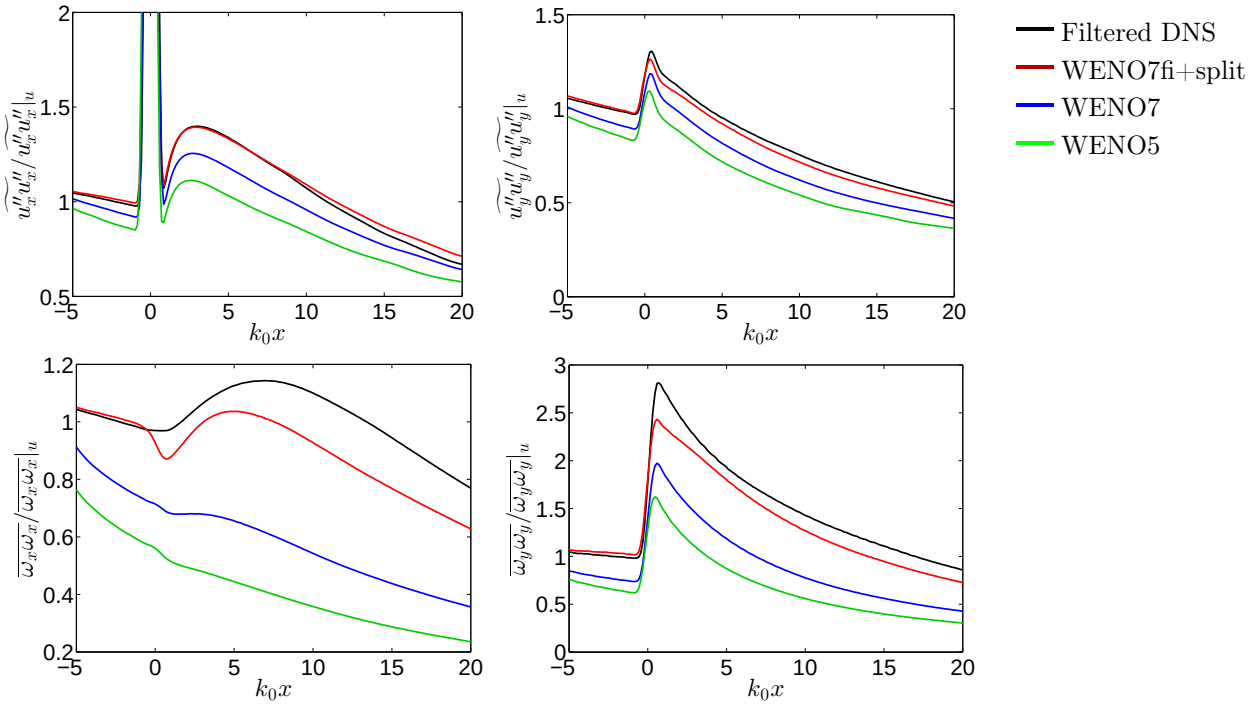

Figure 6: Comparison to filtered DNS data of the statistics obtained by the different numerical schemes (WENO5, WENO7 and WENO7fi+split) on grid 389×64^2, $M = 1.5$. Top row: Reynolds Stress components x (left) and y (right). Bottom row: vorticity components x (left) and y (right). No LES modeling.

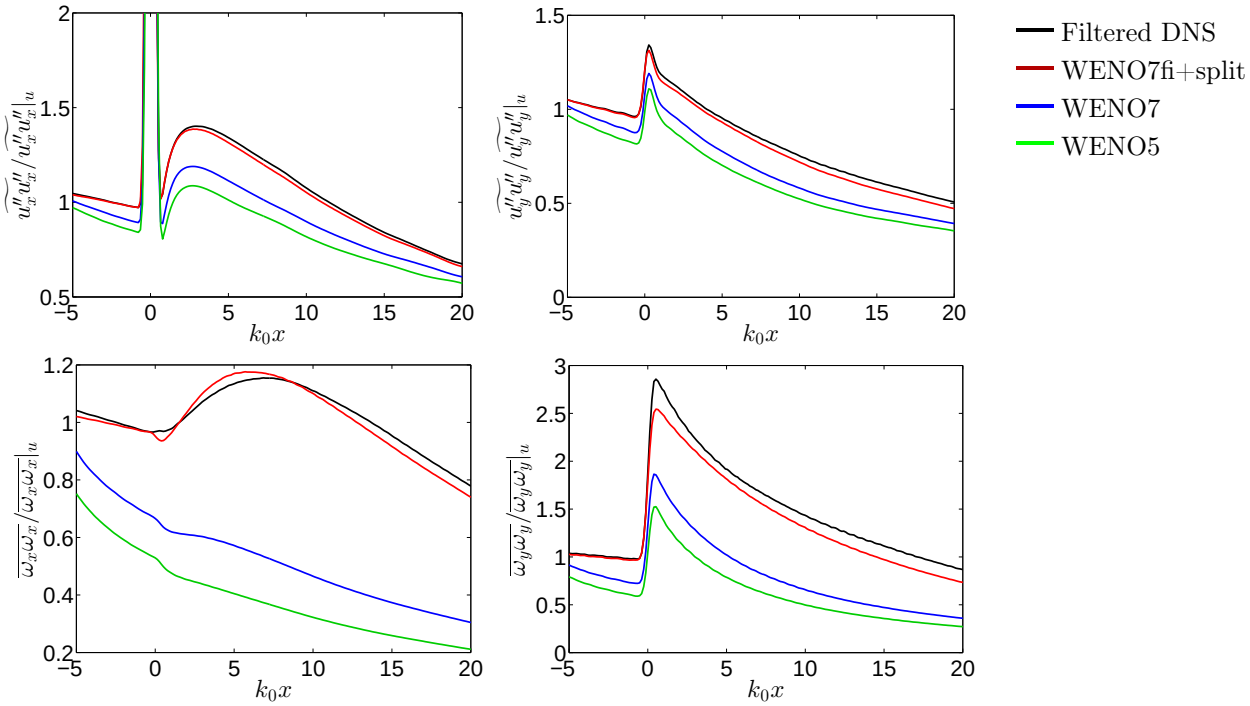

Figure 7: Comparison to filtered DNS data of the statistics obtained by LES using different numerical schemes (WENO5, WENO7 and WENO7fi+split) on grid 389×64^2, $M = 1.5$. Top row: Reynolds Stress components x (left) and y (right). Bottom row: vorticity components x (left) and y (right).

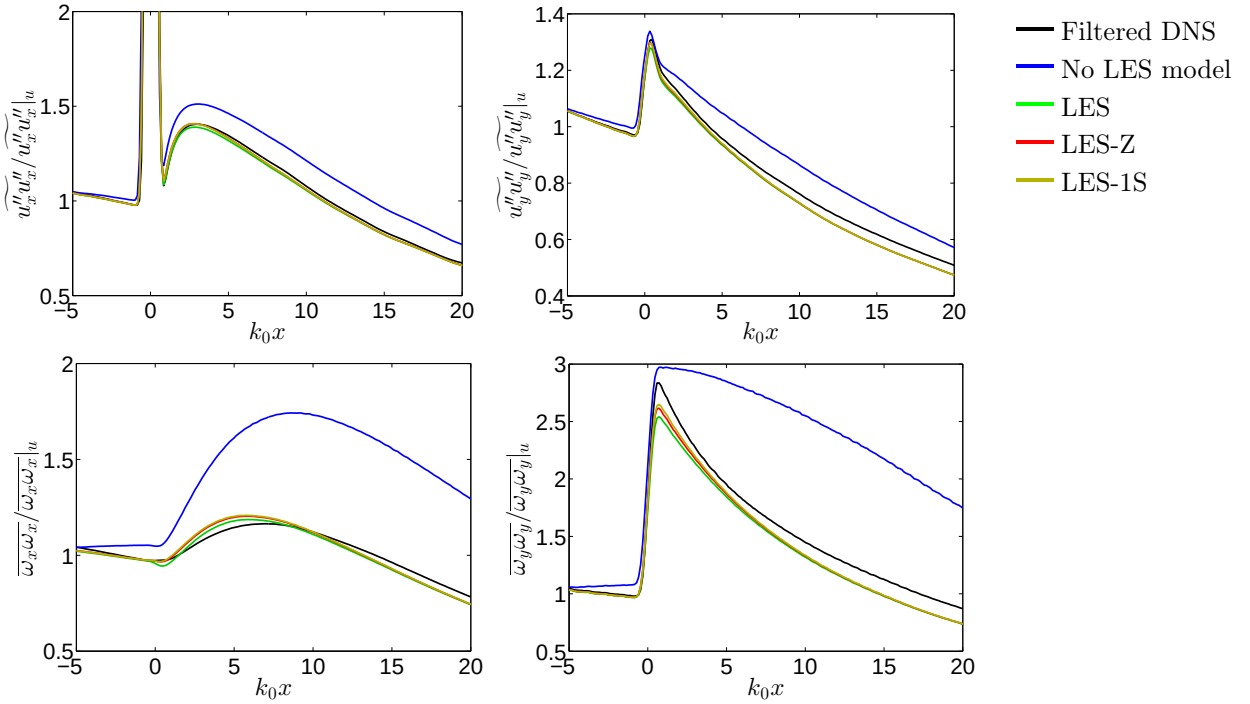

Figure 8: Comparison to filtered DNS data of the statistics obtained by LES with different filtering procedures (standard LES, LES-Z and LES-1S) on grid 389×64^2, $M = 1.5$. Top row: Reynolds Stress components x (left) and y (right). Bottom row: vorticity components x (left) and y (right).

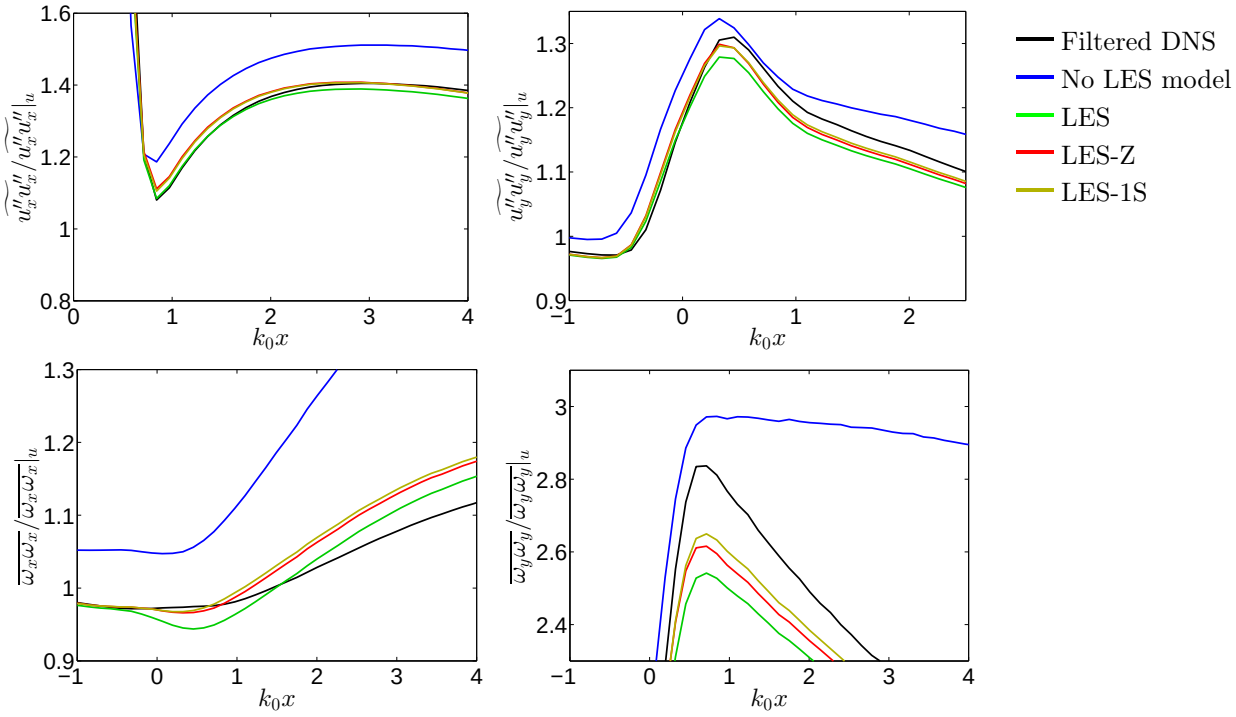

Figure 9: Same as Figure 8, zoom in the vicinity of the shock

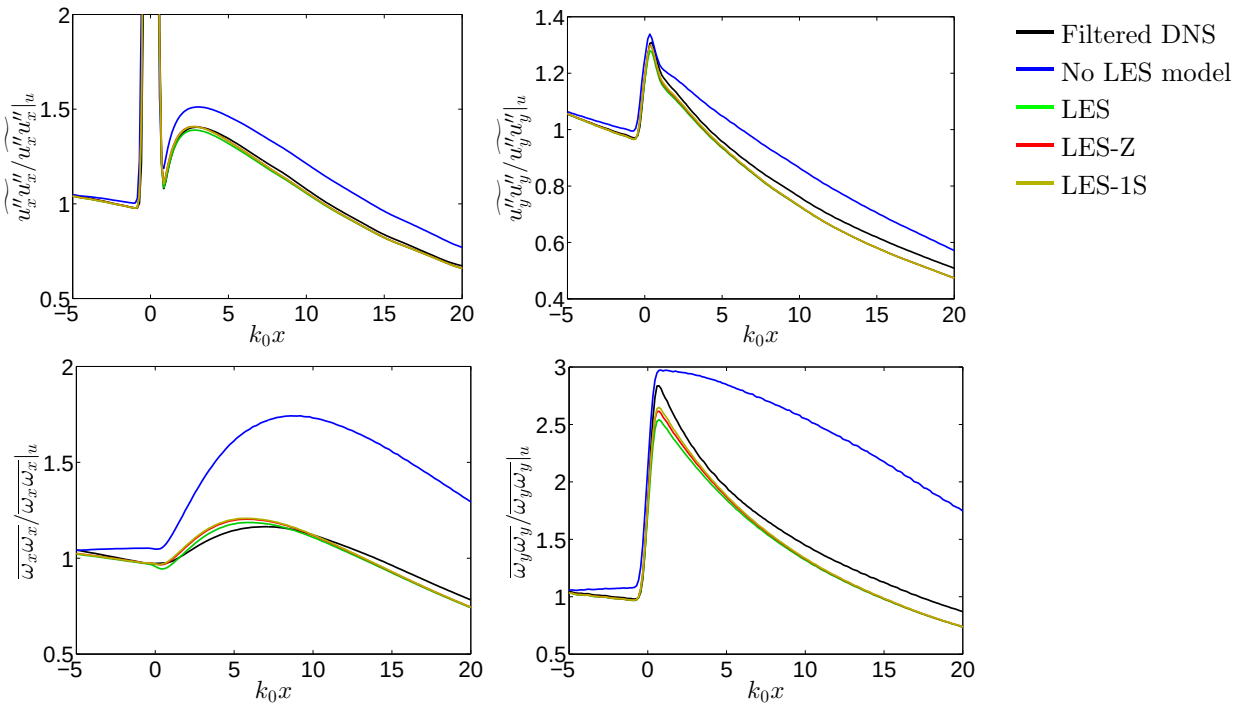

Figure 10: Comparison to filtered DNS data of the statistics obtained by LES with different filtering procedures (standard LES, LES-Z and LES-1S) on grid 777×128^2, $M = 1.5$. Top row: Reynolds Stress components x (left) and y (right). Bottom row: vorticity components x (left) and y (right).

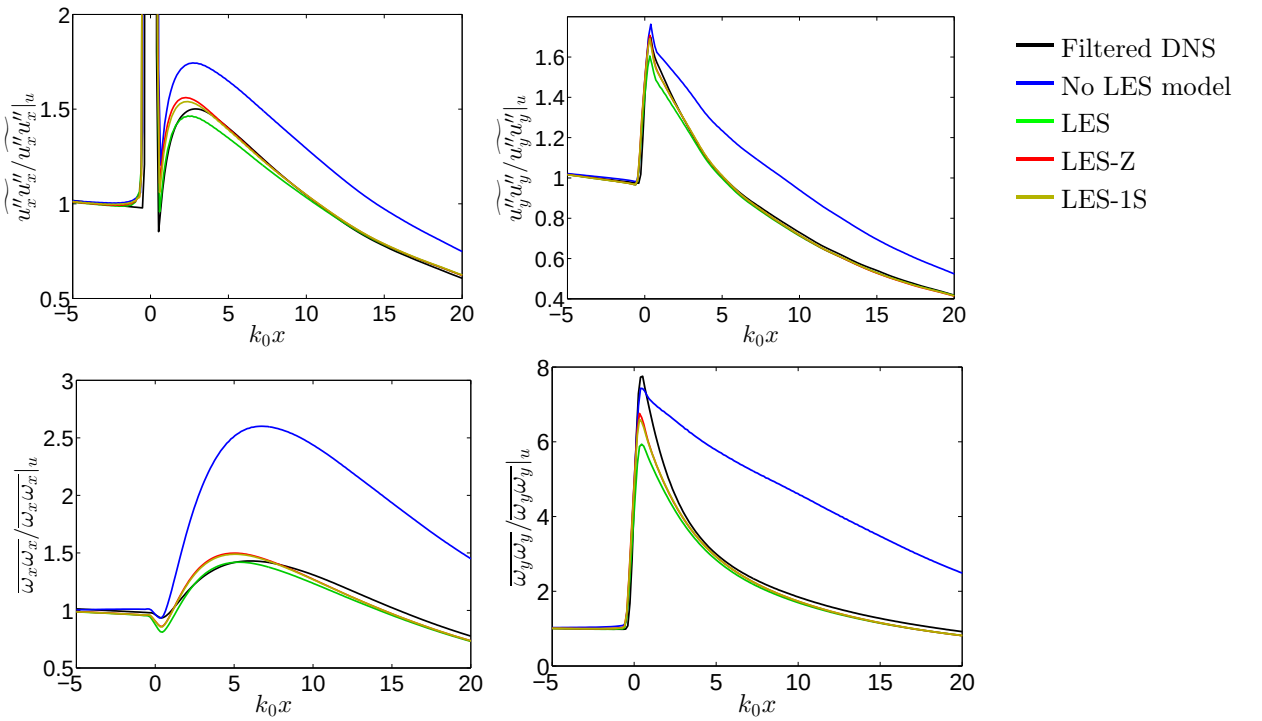

Figure 11: Comparison to filtered DNS data of the statistics obtained by LES with different filtering procedures (standard LES, LES-Z and LES-1S) on grid 389×64^2, $M = 3$. Top row: Reynolds Stress components x (left) and y (right). Bottom row: vorticity components x (left) and y (right).

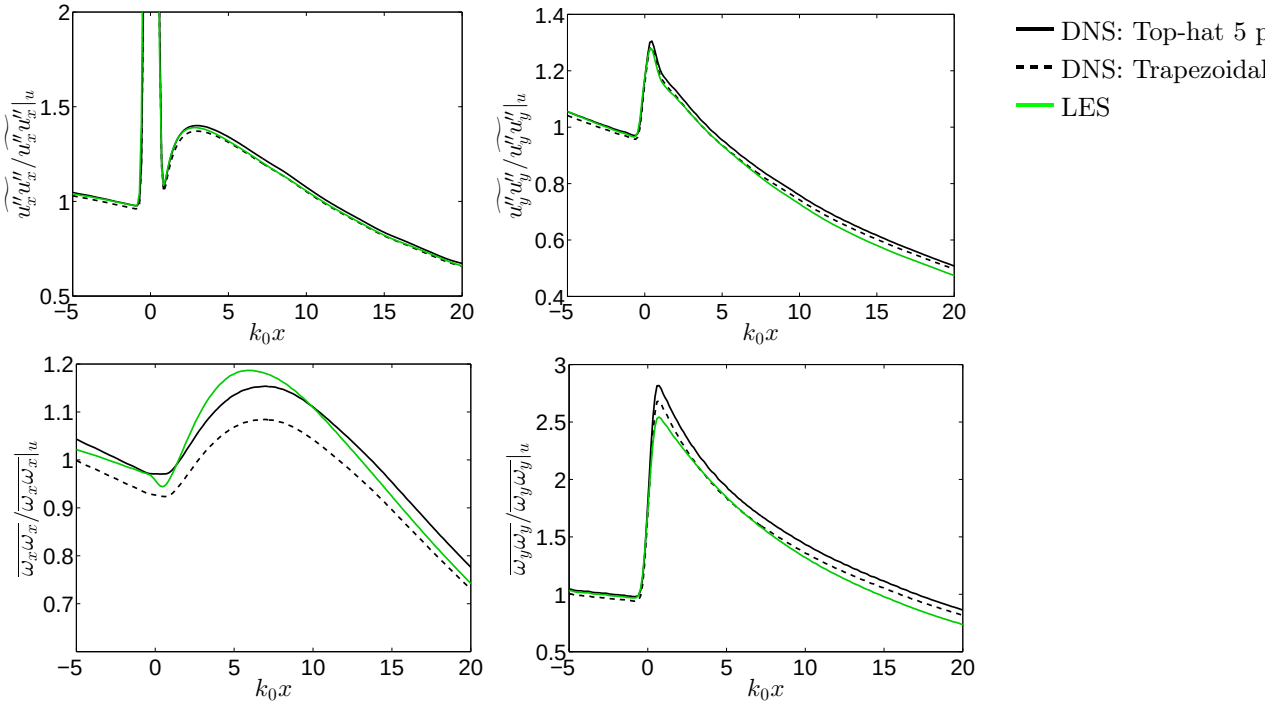

Figure 12: Comparison to filtered DNS data using different filter operator (Trapezoidal and Top-hat). Grid 389×64^2, $M = 3$. Top row: Reynolds Stress components x (left) and y (right). Bottom row: vorticity components x (left) and y (right).